Sulphide Microchemistry and Hydrothermal Fluid Evolution in Quartz Veins, Batouri Gold District (Southeast Cameroon)

SUH Cheo Emmanuel
Economic Geology Unit, Department of Geology and Environmental Science, University of Buea, P.O. Box 63, Buea, S.W. Province, Cameroon. Email: chuhma@yahoo.com

ABSTRACT

Sulphide minerals in the auriferous vein system of the Batouri gold district, southeastern Cameroon, include pyrite, chalcopyrite, sphalerite, galena, covellite and chalcocite. Gold concentrations in these phases reach a high of 0.24 wt% while As and Ag concentrations are quite low when compared to As levels in arsenian pyrite in other gold deposits around the world. These sulphides and the accompanying Au were precipitated from hydrothermal fluids that evolved from primordial H_2O-rich fluids (type 1) into H_2O-CO_2-dominated fluids (type 2) through selective trapping of CO_2 and preferential water loss. Late fluids, probably meteoric in origin (type 3), have no CO_2 and very low homogenization temperatures (< 135°C). Type 3 fluids have extremely low salinities (<1 wt% eq. NaCl) as opposed to the type 1 (<1 to 6.5 wt% eq. NaCl) and the type 2 inclusions (<1 to 8 wt% eq. NaCl). Isochores constructed with FLINCOR show that the peak metamorphic conditions in this region were attained at ~ 550°C and ~ 3.5 kbar. The fluids trapped at this stage progressively lost water and became richer in CO_2. This effect reflects the preferential loss of water in shear zones affected by multistage and episodic quartz recrystallization. The fluid inclusions in this district are similar to carbonic inclusions of world class orogenic gold deposits in other parts of the world thereby indicating that the Batouri district is a favourable region for primary gold exploration.

Keywords: gold, sulphides, hydrothermal fluid, isochores, salinity, Cameroon

RESUME

Les minéraux sulfureux des veines aurifères du district minier de Batouri dans le Sud-Est Cameroun, comprennent la pyrite, la chalcopyrite, la sphalérite, les galènes, la covellite et la chalcocite. Les concentrations en or (Au), dans ces phases minérales atteignent 0,24% en poids d´oxydes alors que celles en arsénic (As) et en argent (Ag) sont faibles par rapport aux concentrations habituelles dans les autres gisements aurifères à travers le monde. Les minéraux sulfureux et l´or associés ont été précipités par des fluides hydrothermaux qui ont évolué de fluides primitifs riches en H_2O (type 1) à des fluides à prédominance de CO_2 (type 2) à travers un piégeage sélectif du CO_2 et préférentiellement une perte en eau. Des fluides tardifs, probablement d'origine météorique (type 3), sont dépourvus de CO_2 et présentent de très faibles températures d'homogénéisation (< 135° C). Les fluides de type 3 présentent extrêmenent de basses salinités (< 1 % poids eq. NaCl) par opposition aux inclusions de type 1 (< 1 à 6,5 % poids eq. NaCl) et de type 2 (< 1 à 8 % poids eq. NaCl). Les courbes isochores construites à partir du logiciel FLINCOR montrent que les pics des conditions métamorphiques dans cette région ont atteint environ 550° C et 3,5 kbar. Les fluides piégés à ce stade ont perdu progressivement de l'eau et se sont enrichis en CO_2. Cette action reflète la perte préférentielle d'eau dans des zones de cisaillement affectées par la recristallisation du quartz à plusieurs niveaux et de façon épisodique. Les inclusions fluides de la région de Batouri sont similaires aux inclusions carboniques des gisements d'or de classe mondiale décrits dans d'autres régions du monde. La région de Batouri peut par conséquent être considérée comme étant une zone favorable à l'exploration de gisements primaires d'or.

Mots clés : or, minéraux sulfureux, fluide hydrothermal, isochore, salinité, Cameroun.

INTRODUCTION

In many mesothermal gold deposits, gold commonly occurs in association with sulphide minerals such as arsenopyrite, pyrite, chalcopyrite, galena and sphalerite (e.g. Genkin et al., 1998). There always has been scientific debate as to whether the gold occurs as colloidal particles in these sulphides (e.g. Chryssoulis and Cabri, 1990) or it is chemically incorporated in the crystal structure of the host sulphide mineral (e.g. Cabri et al. 1989; Asadi et al. 2000). Knowledge on the different modes of gold occurrence transcends pure academic interest as it is also of great importance in designing mineral-dressing procedures. Also the composition of sulphides enables us to compare one mesothermal gold deposit to another. Consequently, the microchemistry of sulphide phases in gold deposits is routinely determined by electron microprobe.

Hydrothermal ore deposits are formed through the deposition of metals from aqueous liquids and vapour (Williams-Jones and Heinrich 2006; Yudovskaya et al. 2006) that circulate within the earth's crust. The precious metal such as gold is often transported as complex ions. As long as the fluids remain thermodynamically stable, the metals also remain in solution (Heinrich 2005). However, if the fluids are caused to boil due to changes in the geothermal regime, or they start cooling as they rise, or they react with wall rock into which the fluids have been channeled, then the metals are precipitated to form ore deposits (Landis and Rye, 2005; Landtwing et al. 2005). Usually crystals forming from these fluids trap tiny droplets of the fluid. These trapped and well preserved fluids are called fluid inclusions and have been widely used in mineral exploration and metallogenetic studies (e.g. Ulrich et al., 1999; Keyahov et al. 2003). By comparing the fluid inclusion characteristics of known hydrothermal deposits to those of poorly studied areas, it is possible to comment on the favourability of exploration in such remote regions.

The Batouri gold district (centred at 14°19'E, 4°27'N; Fig. 1) of eastern Cameroon is an example of a poorly understood gold-bearing hydrothermal vein system along NE-trending shear zones. The primary gold mineralization here occurs as disseminations in hydrothermally-altered granitic wall rock and quartz veins. It is principally the concordant quartz veins that are mineralized. This mineralization is therefore controlled by brittle-ductile structures and the presence

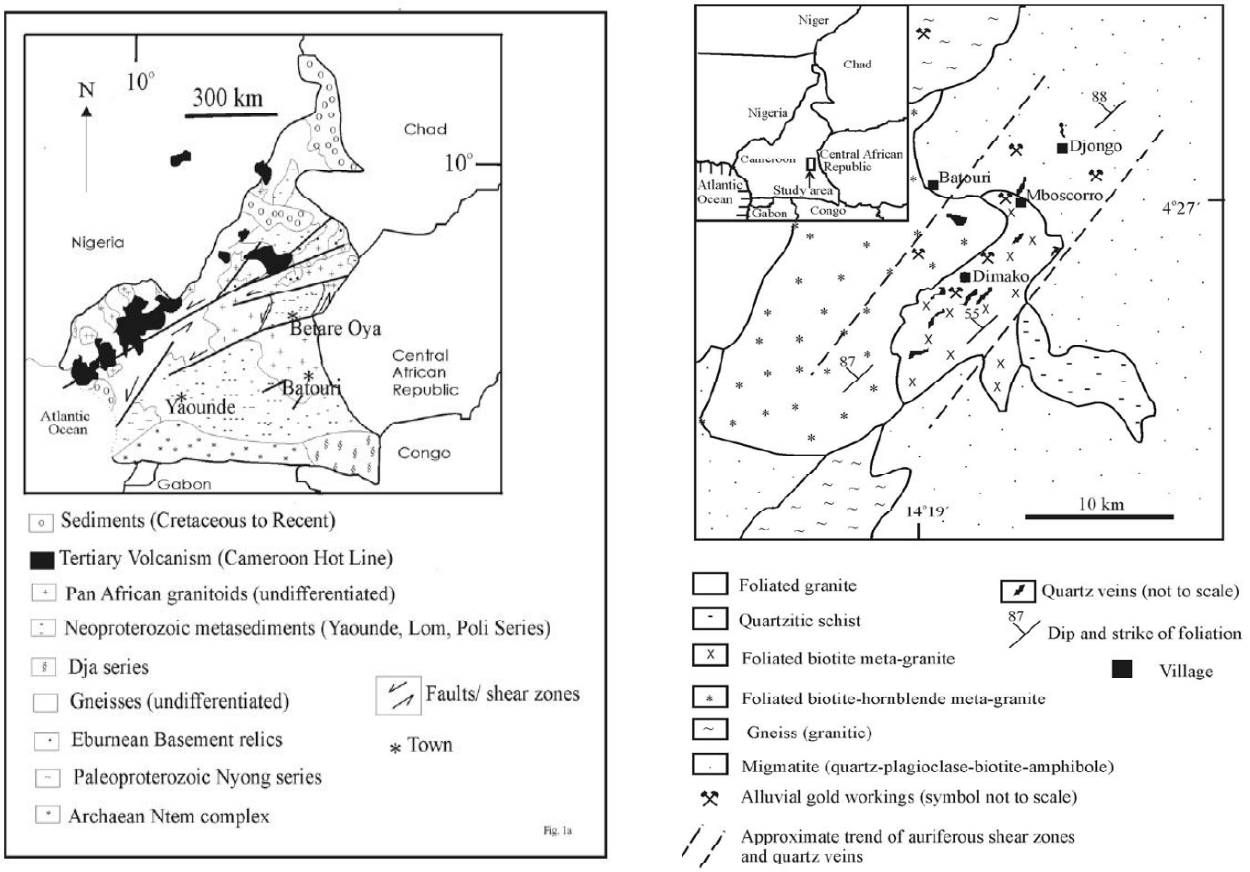

Fig. 1: (a) Geological sketch map of Cameroon showing the location of the Batouri gold district. (b) geological map of the Batouri gold district (modified from Suh and Lehmann 2003).

of these favourable features provides suitable sites for gold concentration. A key aspect in unraveling the metallogenesis of primary gold mineralization in these shear zones is the investigation of the sulphide composition and the nature of fluid inclusions in them. Gold mining in the Batouri district of southeastern Cameroon has been going on for several decades since the 1930s (Suh and Lehmann, 2003). However, most of the mining has been in the hands of small scale miners who target only the readily recoverable gold in stream sediments and weathered quartz veins/ overburden. The primary gold in the unweathered quartz veins is located at great depths and requires industrial scale mining to recover it. Presently, systematic exploration for primary gold in the Batouri district is being carried out by African Aura Resources (AAR), a Toronto stock market listed company based in London. AAR has carried out stream sediment analyses; grid soil analyses as well as exploration pit analyses (see www.african-aura.com for details). Indeed diamond core drilling to evaluate the economic potential of deposits in the district commenced in May 2008. Industrial scale mining demands a good knowledge of the primary mineralization itself in order to optimize exploration costs. Reconnaissance fluid inclusion data for the Batouri area have revealed the presence of CO_2-rich fluids in the gold-bearing quartz veins (Suh et al., 2006). However, these reconnaissance data have two limitations: (i) the fluid inclusion data for the late-stage and barren quartz veins were not provided, and consequently, (ii) isochores to investigate the evolution of the fluids could not be constructed. These issues are addressed in this paper making use of more recently acquired fluid inclusion measurements. Also, a new category of fluid inclusions not described in the earlier study is recognized and documented. To get a better understanding of hydrothermal fluid evolution in this gold district isochores are constructed to show that the initial fluid was a mixture of H_2O and CO_2. It is also demonstrated here that due to post-entrapment modifications, H_2O was progressively lost while CO_2 was preferentially retained. Following the introduction of meteoric water a third class of inclusion that is H_2O-rich was also trapped. These data show that the Batouri

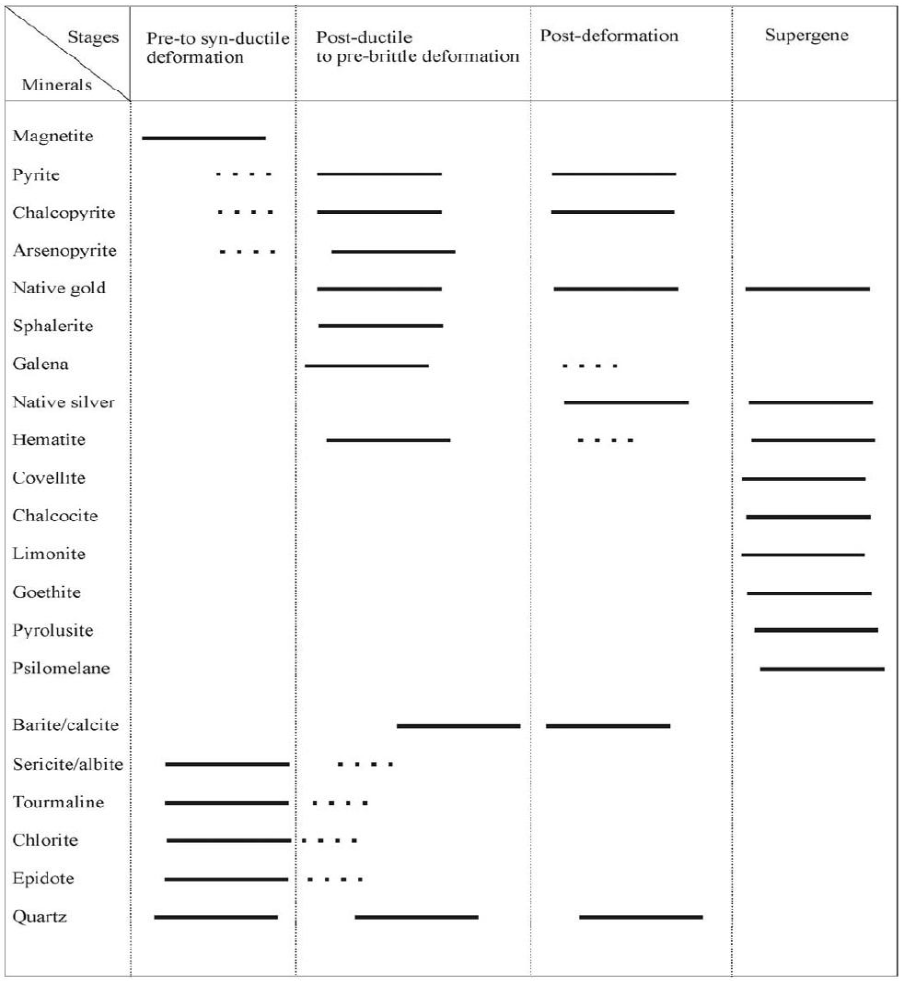

Fig. 2: Mineral paragenesis in the gold-bearing quartz veins of the Batouri gold district, southeast Cameroon. The various stages refer to episodes of deformation in the quartz veins (crack and seal mechanism) starting with ductile deformation and ending in brittle deformation. The supergene stage is linked to the onset of weathering.

district has fluid inclusion characteristics that are similar to other world class gold deposits; a good reason to carry on with primary gold exploration efforts in the region. The microchemistry of the main sulphide phases is also provided and it shows that pyrite has low Au concentration while the high Au concentration in galena and covellite/chalcocite reflects the inclusion of submicrometer-size Au particles in them.

Geological situation and primary gold mineralization

The geology of the Batouri gold district is discussed by Gazel and Gerard (1954) and Suh et al. (2006). Briefly, the mineralization is hosted by quartz veins and quartz/wall rock stringers within shear zones. The host rock is a peraluminous, magnetite series, meta-granite that lies just north of the inferred northern limit of the Congo craton (Fig. 1) and its petrology is discussed elsewhere (Suh et al. 2006). The fresh meta-granite consists of quartz, plagioclase feldspar, biotite and rare hornblende. However, portions of this host rock that have been altered by the hydrothermal fluids are bleached, silicified, ferruginized and carbonitized. Consequently albite, sericite, hematite, calcite, $\pm$ chlorite, $\pm$ epidote, $\pm$ pyrite appear in the mode of the weakly foliated altered rock. These wall rock alteration categories are the main indications of gold concentration in the region. The quartz veins have experienced various crack and seal events starting with a ductile phase in which early quartz grains are drawn out into ribbons, followed by a brittle stage in which vugs were created and later filled by barren undeformed quartz (Suh and Lehmann 2003). The quartz veins are enveloped by sericite- and silica-rich alteration zones which often carry gold (Suh et al. 2006). Gold concentrations reach a high of 53.5 ppm in the quartz veins and 2.6 ppm in the alteration envelop. The fresh, unaltered meta-granite itself is barren and the genetic link between this rock and the ore-bearing quartz veins has not been determined. The main ore minerals in the quartz veins and wall rock are summarized in Fig. 2. Native gold occurs as microscopic inclusions in chalcopyrite and sphalerite which, together with barite, dominate the post-ductile to pre-brittle deformation main ore concentration stage (Fig. 2). The post-deformation sulphides that are vug-filling and euhedral are more abundant in the barren veins. Gold also occurs as free stringers in the gangue quartz matrix and in association with secondary hematite, native silver, covellite, chalcocite, limonite, goethite, pyrolusite and psilomelane (supergene stage; Fig. 2). Typically, the gold grains are a few microns to over 100 microns in size. Due to incipient weathering, the gold grains develop patches with low Ag content (Fig. 3). Overall, the gold is Ag-bearing (< 12.1 wt%, Fig. 3) although Au content can be as high as 100 % Au (Fig. 3).

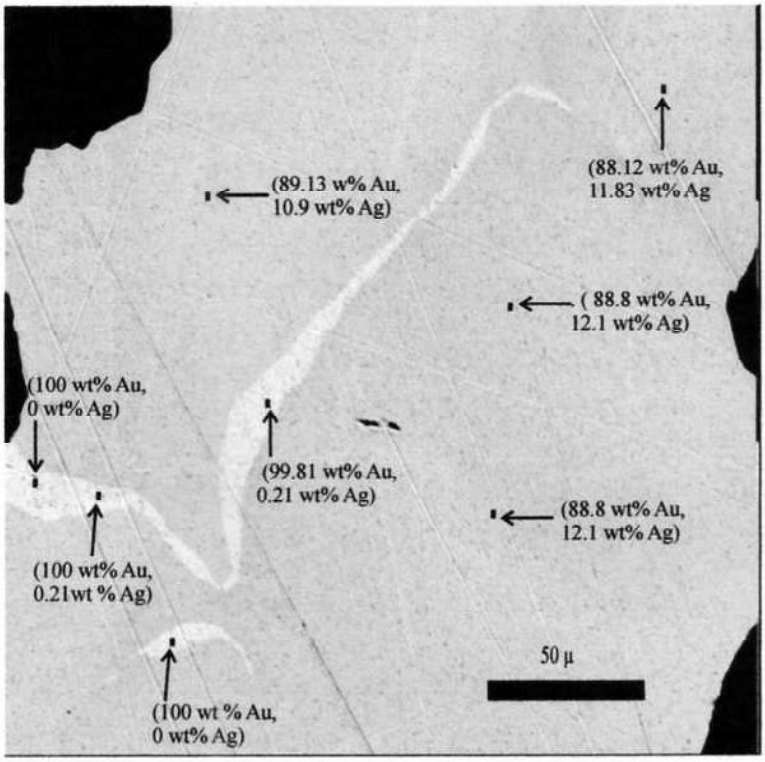

Fig. 2: Backscattered electron image of a typical gold grain in the gold-bearing quartz veins. The relative gold (Au) and silver (Ag) content (in wt %) for different spots of the grain are indicated. Note that Au content in the thin wavy band is higher due to Ag loss as weathering sets in. Image obtained on a Cameca SX 100 electron microprobe operated at 20 Kv, 40 n A using PET crystal with K? lines and counting times of 20 seconds per element. Standards: pure Au and Ag metals.

Field and laboratory methods

Quartz veins within the alteration envelop of the meta-granite were sampled at depths of ~ 15 m from random eluvial gold mining pits that reached the top of the fresh rock. Concordant quartz veins that are gold-bearing as well as discordant, late and barren quartz veins were sampled. The sulphide minerals were analyzed in polished sections by electron microprobe. All sample preparations and analyses were accomplished at the laboratories of the Institute of Mineralogy and Mineral Deposits, Technical University of Clausthal, Germany. The Cameca SX100 electron microprobe used was operated at a beam current of 40 nA and an accelerating voltage of 20 kV. The counting times during the analysis for the concentrations of the elements in each mineral phase were set at 20 seconds per element. The following standards were used: chalcopyrite (for Cu, S and Fe), sphalerite (for Zn), and the synthetic compound GaAs (for As), PbTe (for Pb), barite (for Ba) and pure metallic gold for Au and metallic silver for Ag. The atomic concentrations of elements in each mineral as well as the atomic number of the elements were used to calculate the atomic proportions (stoichiometry) of the minerals using standard procedures. Detection limits were set at ~ 0.02 wt% (Au) and 0.03 wt% (all the other elements). All values below these detection limits are indicated as zero on the data tables.

For the fluid inclusion studies, doubly polished sections were prepared for each sample. These sections were reduced to wafers ~ 33 µ thick, mounted on glass slides, and the nature of the fluid inclusions in them studied under a high magnification transmitted light petrographic microscope. To liberate the wafer from the glass slide, each slide was immersed in acetone for about 10 minutes to dissolve the Canada balsam glue and subsequently rinsed with distilled water several times. Thereafter, each inclusion of interest was then analyzed for its microthermometric data using a United States Geological Survey-type heating freezing stage (Roedder 1984). This stage consists of a high resolution microscope that is equipped with a heating device and connected to a liquid nitrogen tank by a tiny tube. During the freezing runs, liquid nitrogen is passed over the quartz wafer slowly until the inclusion freezes completely (at ~ -100°C). The frozen inclusion is subsequently heated up at a rate of about 0.1°C/second until the ice starts melting. This initial ice melting temperature (Tm ice) is noted. For the CO_2-bearing inclusions, the temperature at which the inclusion finally melts is noted (this is the CO_2 homogenization temperature, Th CO_2). Also, the temperature at which the CO_2 bubble is completely exsolved from the liquid is also noted (CO_2 clathrate). For all the two and three phase inclusions, the heating continued until the vapour and liquid phases of the inclusions homogenized into a single phase (usually into

Table 1: Microchemistry of representative pyrite crystals (wt %) and atomic proportion (%), in the Batouri gold district.

	S	Fe	Ba	Pb	As	Zn	Ag	Cu	Au	Total
Composition										
	52.57	43.4	1.55	1.54	0.47	0.46	0.01	0.01	0	100.01
	49.59	42.01	0.01	5.06	1.57	1.72	0.02	0	0.03	100.01
	52.93	45.09	0	0.04	0	1.93	0	0.01	0	100
	49.91	42.56	0.02	4.26	1.36	1.87	0.01	0.02	0	100.01
	53.17	45.76	0	0.03	0	0.96	0.08	0	0	100
Atomic proportion										Total
	66.96	31.73	_	_	_	_	_	_	_	98.69
	65.24	31.73	_	1.03	_	1.11	_	_	_	99.11
	66.35	32.45	_	_	_	1.11	_	_	_	99.91
	65.22	31.94	_	_	_	1.2	_	_	_	98.36
	66.52	32.86	_	_	_	_	_	_	_	99.38

Table 2: Microchemistry of representative chalcopyrite crystals (wt %) and atomic proportion (%), in the Batouri gold district.

	S	Cu	Fe	Zn	Ba	Pb	Au	Ag	As	Total
Composition										
	35	33.48	28.92	2.43	0.08	0.05	0.03	0.02	0	100.01
	34.87	33.71	29.12	2.15	0.13	0	0	0.03	0	100.01
	34.98	32.9	28.71	3.26	0.11	0	0.04	0	0	100
	34.39	27.11	22.81	15.51	0.05	0.04	0	0.09	0	100
	34.85	33.71	27.61	3.72	0.06	0.05	0	0	0	100
Atomic proportion										Total
	50.21	24.23	23.81	1.71	_	_	_	_	_	99.96
	50.04	24.41	23.98	1.52	_	_	_	_	_	99.95
	50.19	23.82	23.65	2.29	_	_	_	_	_	99.95
	49.98	19.88	19.03	11.05	_	_	_	_	_	99.94
	50.1	24.45	22.79	2.62	_	_	_	_	_	99.96

Table 3: Microchemistry of representative sphalerite crystals (wt %) and atomic proportion (%), in the Batouri gold district.

	Zn	S	Au	Ba	Cu	Ag	Fe	Pb	As	Total
Composition										
	66.29	33.56	0.08	0.03	0.02	0.01	0.01	0	0	100
	64.14	33.88	0	0	0.03	0.23	1.65	0.09	0	100.02
	52.73	28.6	0	0.04	0.04	0.08	2.11	16.39	0	99.99
	61.4	35.17	0	0.57	0.02	0.24	2.41	0.2	0	100.01
	63.47	32.93	0	0	0.03	0.31	3.26	0	0	100
	64.22	32.98	0	0.01	0.01	0.18	2.53	0.05	0.02	100
Atomic proportion										
	49.17	50.77	_	_	_	_	_	_	_	99.94
	47.39	51.05	_	_	_	_	1.43	_	_	99.87
	44.38	49.09	_	_	_	_	2.08	4.35		99.9
	45	52.56	_	_	_	_	2.07	_	_	99.63
	47.14	49.87	_	_	_	_	2.83	_	_	99.84
	47.71	49.97	_	_	_	_	2.2	_	_	99.88
	49.17	50.77	_	_	_	_	_	_	_	99.94

Table 4: Microchemistry of representative galena crystals (wt %) and atomic proportion (%), in the Batouri gold district.

	Pb	S	Zn	Cu	Fe	Ag	Ba	Au	As	Total
Composition										
	83.99	13.58	2.41	0.01	0	0	0	0	0	99.99
	84.26	13.6	2.05	0.08	0	0	0	0	0	99.99
	82.5	13.57	3.82	0	0.07	0	0.04	0	0	100
	79.41	13.49	6.82	0.08	0.13	0	0.03	0.04	0	100
	79.06	13.53	7.07	0.06	0.15	0	0.02	0.11	0	100
	81.41	13.61	4.81	0.03	0.08	0	0.05	0	0	99.99
	61.77	17.41	19.75	0.14	0.89	0	0	0.04	0	100
	84.72	13.06	2.17	0.05	0	0	0.01	0	0	100.01
	83.72	13.53	2.65	0.06	0.02	0	0.01	0.02	0	100.01
Atomic proportions	46.8	48.91	4.26	_	_	_	_	_	_	99.97
	47.09	49.12	3.64	_	_	_	_	_	_	99.85
	45.17	48.03	6.63	_	_	_	_	_	_	99.83
	42.01	46.13	11.43	_	_	_	_	_	_	99.57
	41.65	46.06	11.81	_	_	_	_	_	_	99.52
	43.98	47.53	8.23	_	_	_	_	_	_	99.74
	25.67	46.75	26.01	_	1.37	_	_	_	_	99.8
	48.09	47.92	3.9	_	_	_	_	_	_	99.91
	46.55	48.62	4.67	_	_	_	_	_	_	99.84

Table 5: Microchemistry of representative chalcocite/covellite crystals (wt %) and atomic proportion (%), in the Batouri gold district.

	Cu	S	Zn	Ag	Fe	Au	Pb	Ba	As	Total
Composition										0
	63.75	32.89	2.07	0.45	0.33	0.23	0.15	0.14	0	100.01
	62.86	33.05	2.72	0.64	0.38	0.24	0.02	0.1	0	100.01
Atomic proportions	48.38	49.47	1.53	_	_	_	_	_	_	99.38
	47.64	49.65	2.01	_	_	_	_	_	_	99.3

the liquid phase), and the meniscus between then disappeared. This is known as the total homogenization temperature, Th total.

The isochores were constructed using the standard fluid inclusion computer software FLINCOR based on the equations of state of Brown and Lamb (1989). These equations make use of the proportion of the inclusion occupied by a gas bubble (where there is one), the CO_2 density and the salinity of the fluid inclusions (Brown and Lamb 1989). The salinity of the inclusions was calculated from the final ice melting temperatures while the Th CO_2 was used to calculate CO_2 densities (Roedder 1984).

OBSERVATIONS AND INTERPRETATIONS

Sulphide microchemistry

The results of the microprobe analyses of the main sulphide minerals in the Batouri gold district are presented in Tables 1 - 5. The stoichiometry of pyrite

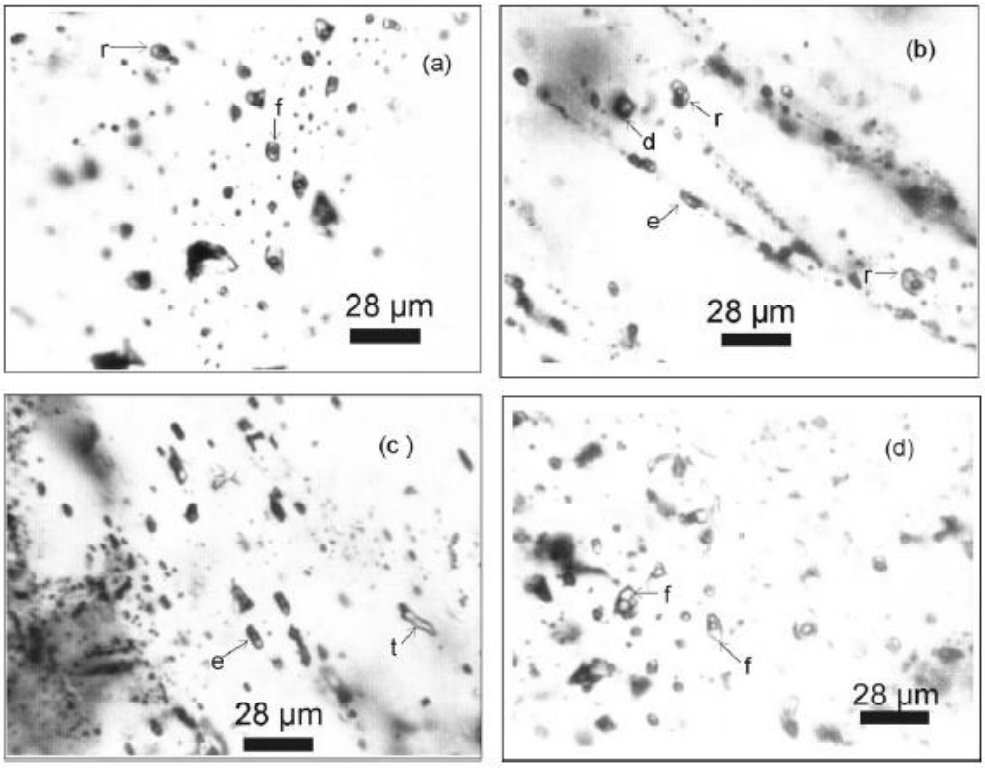

Fig. 4: Photomicrographs of typical fluid inclusions in quartz vein samples. Note the vapour bubble in most inclusions. (a) faceted 'negative crystal' (f), rounded with slender neck (r), and irregular shape fluid inclusions (types 1 and 2) defining a linear array within a single quartz crystal; (b) rounded (r), diamond-shaped (d), elongated (e), and dot-like (tiny dark specks) fluid inclusions (type 2) along a transgranular microfracture; (c) elongated (e) and tubular necked-down (t) fluid inclusions (type 2) along intragranular microfractures; (d) randomly distributed clusters of faceted, rounded and irregular type 3 fluid inclusions within an individual quartz crystal.

as determined from atomic proportions is FeS_2 and it has 0.47 - 1.57 wt% As and very low Au content reaching a maximum value of 0.03 wt% (Table 1). Pb and Zn appear in significant amounts in some of the pyrite analyses as impurities. The chalcopyrite microchemistry (Table 2) indicates that Zn is present in the mineral besides the expected Cu, Fe and S. This probably reflects limited replacement of Fe and Cu by Zn. The chalcopyrite analyses also indicate 0.03 - 0.04 wt% Au but As is totally absent. Sphalerite analyses (Table 3) and galena analyses (Table 4) revealed that these phases may have as much as 0.08 wt% Au and 0.11 wt% Au, respectively. The covellite / chalcocite minerals have high Au concentrations (0.23 - 0.24 wt% Au) in them (Table 5). Ag and As concentrations in sphalerite, galena and covellite are low.

Fluid inclusion characteristics

The typical morphologies of the fluid inclusions from the quartz vein samples are illustrated in Figure 4. All the inclusions are secondary in nature since they either follow trails (healed fractures, growth planes and cleavage planes in the crystals) or are scattered within the late quartz grains. These inclusions are mostly two phase inclusions (liquid and vapour) although some of the carbonic inclusions have three phases (liquid: immiscible water and carbon dioxide, and a CO_2 vapour) (Fig. 4). Monophase carbonic inclusions are also widespread. Based on the host vein and petrographic characteristics the fluid inclusions can be divided into three main types. Type 1 (usually < 2 - 20µ) inclusions are mainly intragranular and may follow growth zone boundaries within a single grain or be randomly scattered within the grain. Type 2 (commonly < 2 - 25µ) inclusions mainly follow intergranular trails healing microfractures that run through several grains within the same sample. Type 3 inclusions are typically large (15 - 33µ), irregular in outline, and occur as interstitial as well as random intragranular clusters. These type 3 inclusions have not been described before and are therefore given greater attention here. Types 1 and 2 inclusions occur in the gold-bearing quartz veins while the type 3 inclusions are typical of the barren and late quartz veins.

The microthermometric data for the three categories of fluid inclusions are summarized in Table 6. Microthermometric data for the type 1 inclusions

Table 6: Summary of fluid inclusion data on quartz vein samples from the Batouri gold district.

Fluid inclusions		Microthermometric data						
Class		Tm CO_2	Th CO_2	Tm ice	T clathrate	Th total	**Salinity	CO_2 density
Class 1	Subtype (i)	(-62.8 to -52.1) (x = -57.7) (s.d. = 2.52) (n = 16)	(-32 to -9.2) (x = -22.75) (s.d. = 7.77) (n = 16)	(-5.9 to -2.88) (x = -4.08) (s.d. = 1.20) (n = 9)	(6 to 11.6) (x = 7.69) (s.d. = 1.53) (n = 16)	(275.3 to 333) (x = 301.19) (s.d. = 21.19) (n = 9)	(<1 to 8) (x = 4.49) (s.d. = 2.61) (n = 11)	(0.98 to 1.09) (x = 1.05) (s.d. = 0.06) (n = 11)
	Subtype (ii)	(-62.1 to -52.1) (x = -56.77) (s.d. = 1.38) (n = 41)	(-8.8 to 28.5) (x = 5.80) (s.d. = 14.16) (n = 41)	(-5.6 to -2.1) (x = -3.42) (s.d. = 1.13) (n = 21)	(6.1 to 11.5) (x = 8.36) (s.d. = 1.45) (n = 42)	(275 to 343.1) (x = 301.31) (s.d. = 22.34) (n = 21)	(<1 to 7.8) (x = 4.02) (s.d. = 2.19) (n = 29)	(0.65 to 0.98) (x = 0.89) (s.d. = 0.17) (n = 11)
Class 2	Subtype (i)	(- 57.7 to -56.9) (x = -57.6) (s.d. = 0.66) (n = 3)	(-5.9 to 2) (x = -2.8) (s.d. = 4.2) (n = 3)	(-4.3 to -1.5) (x = -2.08) (s.d. = 0.95) (n = 8)	(9.9 to 10.9) (x = 10.3) (s.d. = 0.53) (n = 3)	(251.1 to 350) (x = 298.85) (s.d. = 35.85) (n = 8)	(<1 to 1.5) (x = 1.06) (s.d. = 0.18) (n = 8)	(0.92 to 0.97) (x = 0.94) (s.d. = 0.02) (n = 8)
	subtype (ii)	Not detectable	Not detectable	(-2.1 to 0.3) (x = -0.04) (s.d. = 0.98) (n = 7)	Not detectable	(241 to 329.3) (x = 281.94) (s.d. = 43.59) (n = 5)	(<1 to 1) (x = 0.98) (s.d. = 0.01 (n = 16)	Not detectable
Class 3		Not detectable	Not detectable	(-1.1 to 0) (x = -0.9) (s.d. = 0.45) (n = 9)	not detectable	(135 to 292.7) (x = 235) (s.d. = 63) (n = 9)	(<1 to ~1) (x = 0.33) (s.d. = 0.09) (n = 9)	Not detectable

T m CO_2 = initial CO_2 melting temperature; Th CO_2 = CO_2 homogenization (to liquid) temperature; Tm ice = final ice melting temperature;
T clathrate = CO_2 clathrate final melting temperature; Th total = final total homogenization temperature. All temperature values in °C.
CO_2 density (in g/cm^3) is determined from Th CO_2 values. x = mean; s.d. = standard deviation at 1 sigma; n = number of analyses.
* Subtypes (i) and (ii) are based on microthermometric data only (CO_2 density for class 1 and presence or lack of CO_2 in class 2). See text for details.
**Salinity calculated with FLINCOR software based on the equations of Brown and Lamb (1989).

indicate that they can be subdivided into two categories (Table 6) on the basis of CO_2 data. In the first category (subtype 1i) where CO_2 is present, CO_2 density is 0.94 $\pm$ 0.02 g/cm^3 and, Tm CO_2 ranges from -57.7°C to -56.9°C. In the second category (subtype 1ii, Table 6), no microthermometric evidence for the existence of CO_2 in the inclusions was obtained. Their Tm ice values are low, -2.1°C to 0.3°C and Th total falls between 241°C and 329.3°C. Type 1 inclusions have very low salinity (<1 to 1.5 wt% eq. NaCl, Table 6).

The type 2 inclusions can also be subdivided into two subtypes based on CO_2 density (Table 6). These type 2 inclusions have slightly higher salinities (4.49 + 2.61 wt% eq. NaCl for high density CO_2 fluids, and 4.02 + 2.19 wt% eq. NaCl for those with slightly lower CO_2 density) and the predominance of Tm CO_2 values at -56.6°C point to the presence of pure CO_2 in these inclusions. Both types 1 and 2 inclusions can therefore be regarded as aqueous-carbonic inclusions (Wille and Klemd, 2004) since they contain H_2O and CO_2. However, the fact that the type 2 inclusions have higher salinities indicates that they have lost a significant amount of H_2O compared to the type 1 inclusions. For the types 1 and 2 inclusions that have vapour bubbles, the bubbles have a wide range of sizes resulting in variable

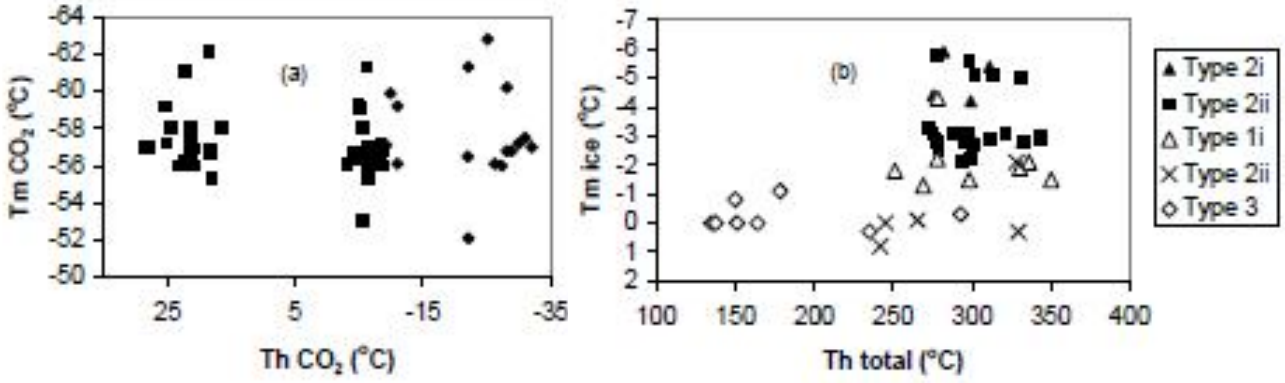

Fig. 5: (a) Th CO2-Tm CO2 diagram for representative carbonic inclusions, (b) Tm-Th diagram for representative fluid inclusions, Batouri gold district, south east Cameroon.

liquid/vapour ratios (see Fig. 4). This is taken to be indicative of fluid immiscibility during the evolution of the hydrothermal fluids. Normally, fluid inclusions that have not undergone immiscibility will have very similar liquid/vapour ratios.

The type 3 inclusions have very unique microthermometric data. They have a restricted Tm ice range, -1.1°C to 0°C. The total homogenization temperatures range from 135°C to 292.7°C. The very low homogenization temperatures for most of these type 3 inclusions indicate that they are late, externally derived, aqueous fluids probably mixed with meteoric water, and cannot therefore be directly related to the mesothermal system. This is a very poignant contribution to exploration in this region as quartz veins in which type 3 inclusions dominate are not worth further exploration.

The microthermometric data for the three classes of inclusions are presented in Figure 5. The inclusions for each type plot in very distinct zones highlighting the different hydrothermal fluid evolution stages that they represent. The type 2 inclusions actually show a bimodal population on the Tm CO_2 versus Th CO_2 plot (Fig. 5a). This bimodal population is related to the effect of hydrothermal fluid unmixing or immiscibility wherein a once homogenous fluid separated into two immiscible fractions upon cooling. The type 3 inclusions predominantly fall at the low Tm ice - Th total range (Fig. 5b).

DISCUSSION

The characteristics of quartz veins and altered wall rock in the Batouri gold district are suggestive of structurally-controlled lode gold mineralization in the deep transitional brittle/ductile deformation domain. The gold-bearing quartz veins here have pyrite, chalcopyrite, sphalerite, galena and covellite/chalcocite as the main sulphide minerals. The pyrite is particularly poor in Au and has very low As content when compared to As concentrations of up to 4.39 wt% in Carlin-type gold deposits (Simon et al. 1999). This suggests a limited degree of As and Au subsitution for Fe in pyrite and may account for the paucity of arsenopyrite in this gold district when compared to similar mesothermal gold deposits (Genkin et al. 1998). Interestingly, high Au concentrations are encountered in the chalcocite and covellite association as well as in galena. There are no experimental data that demonstrate that Au can substitute for Cu in covellite or Pb in galena. Therefore the high Au content in these phases suggests that Au is present in them as submicrometer-size gold particles. In highly weathered mesothermal gold deposits, primary gold is often mobilised and reprecipitated with supergene minerals such as covellite, colloidal hematite and chacocite (Colin and Vieillard, 1991). During such supergene alteration of gold-bearing veins, Au is transported as a bisulfide complex and eventually precipitated as high purity gold. The high Au values (0.23 - 0.24 wt% Au) in chacocite and covellite in this study is interpreted to represent the secondary concnetration of Au as very fine particles around these supergene minerals.

Three categories of fluid inclusions are recognized in quartz veins of the Batouri gold district. Types 1 and 2 inclusions are H_2O-CO_2-bearing and are rampant in the auriferous veins, while the type 3 inclusions contain no CO_2, have very low salinities and low total homogenization temperatures and they are found in the barren veins. The types 1 and 2 inclusions must therefore be related to the parental ore-forming fluid. Such fluids have been demonstrated to have deep crustal origins related to metamorphic devolatization (Dipple and Ferry 1992). Carbonic fluids of this nature point to the presence of deep shear zones which are undoubtedly favourable sites for ore concentration. These inclusions also experienced modifications after entrapment. The type 1 inclusions have more H_2O than the type 2 inclusions and are clearly the oldest generation of fluid inclusions judging from their textural characteristics: they occur only within individual grains; they do not extend across grain boundaries and only follow growth zones in a given crystal. To know how these type 1 inclusions eventually evolved and underwent H_2O loss and post-entrapment modifications, isochores for the various inclusion categories were made from the microthermometric data presented above (Fig. 6). The H_2O-rich (type 1) inclusions are representative of fluids trapped early at peak conditions of ~ 3 to ~ 4.5 kbar and ~ 400-550°C. These inclusions were then modified as a result of quartz (re)crystallization, microfissuring, and partial water leakage leading to the formation of type 2 inclusions which are poorer in H_2O but richer in CO_2 than the type 1 inclusions. This H_2O loss due to the repeated crack-seal mechanism (Ramsay 1980, Urban et al. 2006) is responsible for the large spread of CO_2 densities (Table 6) in these fluid inclusions. Post-entrapment modification of the type 1 fluid inclusions is also inferred from the necking-down features of some of the inclusions (e.g. Fig. 4c, inclusion t). The evolution of the hydrothermal fluid in this system did not follow the isochore defined by the early type 1

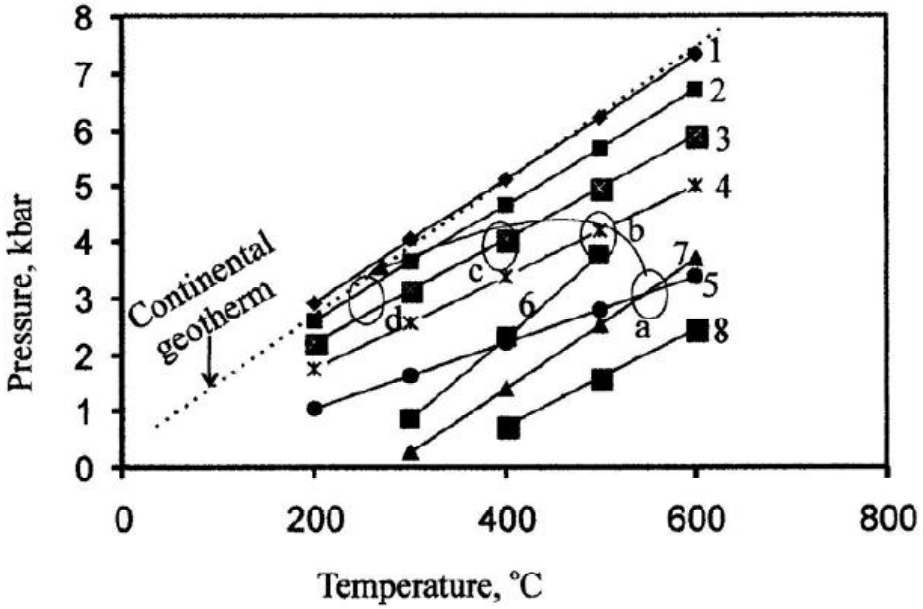

Fig. 6: (P-T diagram showing trapping conditions and fluid evolution within the Dimako-Mboscorro gold system. Isochores for type 3 inclusions that have been diluted by externally derived, possibly meteoric, fluids are not shown because they lie along the continental geotherm. 1 and 2 are isochores for type 2 carbonic inclusions based on the following microthermometric measurements: Isochore 1: Th CO2 = -32°C; salinity = 7.48 wt% eq. NaCl, CO2 density = 1.09 g/cm3. Isochore 2: Th CO_2 = -22.8°C, salinity = 0.81 wt% eq. NaCl, CO_2 density = 1.05 g/cm3. Isochores 3, 4, and 5 are for type 2 inclusions with lower CO_2 density (0.98 g/cm3 and 7.31 wt% eq. NaCl, 0.89 g/cm3 and 3.27 wt% eq. NaCl, and 0.65 g/cm3 and 0 wt% eq. NaCl, respectively), and Th CO_2 values of -8.8°C, 5.8°C and 28.5°C, respectively. Isochore 6 (salinity = 0.98 wt% eq. NaCl, Th total = 241°C), isochore 7 (salinity = 0.98 wt% eq. NaCl, Th total = 281.9°C), and isochore 8 (salinity = 0.98 wt% eq. NaCl, Th total = 329.3°C) correspond to the H_2O-rich type 1 inclusions. The intersections of isochores 4 and 6 as well as isochores 5 and 6, and 5 and 7, give a peak P-T range of ~400 - 550°C and ~3 - 4.5 kbar. The arrow indicates the evolution path of the inclusions (through the ellipses labelled a, b, c, and d) with progressive water loss and CO_2 enrichment. The ellipses a and b represent peak conditions, c marks conditions of limited H_2O leakage, while d corresponds to very dense CO_2 inclusions with extensive H_2O loss and retrograde greenschist facies conditions.

inclusions (Fig. 6), thereby instigating a pressure difference between the inclusions and their surroundings (lithostatic pressure). In response, the fluid inclusions re-equilibrated, and followed a regime of isobaric cooling (Fig. 6) accompanied by substantial water loss, since water is much more mobile due to the higher polarity of its molecules compared to carbon dioxide (van den Kerkhof and Thiery, 2001). The modified inclusions were consequently enriched in dense CO_2 (type 2 inclusions) and experienced volume shrinkage. The H_2O lost contributed to the formation of the low-temperature retrograde mineral assemblage (white mica, chlorite, and epidote) within the proximal areas of the wall rock in the Batouri area. During this low temperature metamorphism accompanied by uplift, meteoric water percolated downwards through the shear zone and mixed with the residual fluids leading to the formation of the type 3 inclusions. This explains why the type 3 inclusions are unusually large, contain no CO_2 and have low salinities. This type 3 inclusions mark the late stages in the tectonic evolution of the shear zone and consequently are common in the late stage quartz veins that carry no gold. Therefore, the interpretation of the fluid inclusion data is consistent with a scenario in which fluids were trapped under peak conditions, as well as during the various stages of ductile and brittle deformation of the quartz vein material, and during the subsequent retrograde event. Indeed, the distribution, and the wide variation in the melting and the homogenization temperatures, even for fluid inclusions within the same category, actually indicate that the fluids were not trapped at the same time, and have also undergone modifications induced by differences in the fluid inclusions internal pressure, lithostatic pressure and quartz recrystallization/grain boundary migration (Bakker and Jansen 1991).

The study of fluid inclusions is always faced with the question of how the inclusions developed the various characteristics they display. Specifically, are the features due to phase separation, unmixing due to boiling and heterogeneous trapping, or they only reflect post-entrapment modifications? Ramboz et al. (1987) postulated from thermodynamic considerations that inclusions with variable liquid/vapour ratios should be the result of fluid immiscibility during hydrothermal fluid evolution. In this study, type 1 and type 2 fluid inclusions coexist even though they represent different

stages in the evolution of the fluid (see Fig. 4a for example). The type 2 inclusions were derived from type 1 inclusions due to selective removal of water (leakage). The variable liquid/vapour ratio in our samples is proving that fluid immiscibility took place during the early stages of the hydrothermal fluid evolution. Fluid immiscibility is a viable mechanism for gold precipitation from fluids along shear zones (e.g. Klein et. 2006 and older references therein). These types 1 and 2 are therefore the parental ore-forming fluids in this gold district.

Aqueous and carbonic fluid inclusions similar to those described in this study have been observed at various mesothermal and orogenic lode gold deposits in the world. Yao and Robb (2000) described carbonic inclusions around the Ashanti gold field of Ghana. Fan et al. (2003) have also described H_2O-CO_2 $\pm$ CH_4 fluids at the Jiandong gold province, China. Other more recent studies in which the ore-forming fluid is CO_2-bearing include Klein et al. (2006) in the Gurupi gold belt of Brazil; Dreher et al. (2008) in Carajas province, Brazil; Pollard (2006) for intrusion-related gold deposits around the world; Urban et al. (2006) in quartz-stibnite veins and Tsige (2006) in the gold veins of the Adola region, Ethiopia. These studies have underpinned the role of this aqueous low salinity (usually < 8 wt% eq. NaCl) and carbonic fluids in the genesis of world class hydrothermal deposits. They have also demonstrated that carbon dioxide densities increase in inclusion with greater H_2O loss as also documented in this study. The similarity in fluid inclusion types at the Batouri gold district and these examples of world class deposits therefore encourages the exploration for primary gold deposits in the Batouri district.

CONCLUSIONS

The conclusions from this study of sulphide mineral composition and hydrothermal fluid evolution within quartz veins of the Batouri gold district can be summarized as follows:

1. 'Invisible' gold (i.e. chemically bound Au in the crystal structure of the sulphide) is absent in the sulphide minerals of this gold district as reflected in the low concentrations of Au in pyrite and chalcopyrite. Rather free gold as submicroscopic metallic particles is inferred to exist in galena and chalcocite/covellite as inclusions.
2. The gold-bearing quartz veins have two main types of fluid inclusions: type 1 inclusions that are H_2O-rich but also contain CO_2; and type 2 inclusions which are essentially carbonic and have high CO_2 densities. Type 2 inclusions evolved from type 1 inclusions through selective water leakage. These fluids are parental to the ore-forming fluid.
3. The third type of inclusion (type 3) has very low salinities and represents percolated meteoric water. This category is common in the barren quartz veins.
4. The similarities between the sulphide microchemistry and fluid inclusions studied here and other carbonic inclusions from world class lode gold deposits are good indicators that the potential exists of finding economic primary gold deposits in the Batouri gold district.

ACKNOWLEDGEMENTS

This work was financed by a Research fellowship of the Alexander von Humboldt Foundation, Bonn, with the support of Prof. Dr. Bernd Lehmann of the Technical University of Clausthal, Germany. Dr. Van den Kerkhof is gratefully acknowledged for his assistance with the interpretation of the fluid inclusion data. Support from the University of Buea through research leave of absences is also acknowledged.

REFERENCES

Asadi, H.H., Voncken, J.H.L and Hale, M. (2000): Sulphosalts at Zarshuran Carlin-like gold deposit, northwest Iran: implications for gold mineralization. *Transactions, Institution of Mining and Metallurgy* (Section B: Applied Earth Science), 110, B24-BB32.

Bakker, J. and Jansen, B.H. (1991): experimental post-entrapment water loss from synthetic CO_2-H_2O inclusions in natural quartz. *Geochimica et Cosmochimica Acta*, 55, 2215-2230.

Brown, P.E. and Lamb, W.M. (1989): P-V-T properties of fluids in the system H_2O ± CO_2 ± NaCl: new graphical presentations and implications for fluid studies. *Geochimica et Cosmochimica Acta* 53, 1209-1221.

Cabri, L.J., Chryssoulis, S.L., De Villiers, J.P.R., Laflamme, J.H.G. and Buseck, P.R. (1989): The nature of 'invisible' gold in arsenopyrite. *Canadian Mineralogist*, 27, 3-362.

Chryssoulis, S.L. and Cabri, L.J. (1990): Significance of gold mineralogical balances in mineral processing. *Transactions of the Institution of Mining and Metallurgy* (Section C: Metallurgy), 99, C1-C10.

Colin, F. and Vieillard, P. (1991): Behaviour of gold in the lateritic equatorial environment: weathering and surface dispersion of residual gold particles, at Dondo Mobi, Gabon. *Applied Geochemistry*, 6, 279-290.

Dipple, G.M. and Ferry, J.M. (1992): Metasomatism and fluid flow in ductile fault zones. *Contributions to Mineralogy and Petrology*, 112, 149-164.

Dreher, A.M., Xavier, R.P., Taylor, B.E. and Martini, S.L. (2008): New geologic, fluid inclusion and stable isotope studies on the controversial Igarape Bahia Cu-Au deposit, Carajas province, Brazil. *Mineralium Deposita*, 43, 161-184.

Fan, H.R., Zhai, M.G., Xie, Y.H. and Yang, J.H. (2003): Ore-forming fluids associated with granite-hosted gold mineralization at the Sanshandao deposit, Jiaodong gold province, China. *Mineralium Deposita*, 38, 739-750.

Gazel, J. and Gérard, G. (1954): Carte géologique de reconnaissance du Cameroun au 1/500 000, feuille Batouri-Est avec notice explicative, Memoir Direction Mines Géologie, Yaoundé Cameroun, 43p.

Genkin, A.D., Bortnikov, N.S., Cabri, L.J., Wagner, F.E., Stanley, C.J., Safonov, Y.G., Mcmahon, G., Friedl, J., Kerzin, A.L. and Gamyanin, G.N. (1998): A multidisciplinary study of invisible gold in arsenopyrite from four mesothermal gold deposits in Siberia, Russian Federation. *Economic Geology*, 93, 463-487.

Heinrich, C.A. (2005): The physical and chemical evolution of low- to medium-salinity magmatic fluids at the porphyry to epithermal transition: a thermodynamic study. *Mineralium Deposita*, 39, 864-889.

Keyahov, R., Bogdanov, K., Fanger, L., von Quadt, A., Pettke, T. and Heinrich, C.A. (2003): The fluid chemical evolution of the Elatiste porphyry Cu-Au-PGE deposit, Bulgaria. (In): Eliopoulos, D.G. (editor), Mineral exploration and sustainable development. Rotterdam, Millpress, p. 1173-1176.

Klein, E.L., Harris, C., Renac, C., Giret, A., Moura, C.A.V. and Fuzikawa, K. (2006): Fluid inclusion and stable isotope (O,H,C, and S) constraints on the genesis of the Serrinha gold deposit, Gurupi belt, northern Brazil. *Mineralium Deposita*, 41, 160-178.

Landis, G.P. and Rye, R.O. (2005): Characterisation of gas chemistry and noble-gas isotope ratios of inclusion fluids in magmatic-hydrothermal and magmatic-steam alunite. *Chemical Geology*, 215, 155-184.

Landtwing, M.R., Heinrich, C.A., Pettke, T., Halter, W.E., Redmond, P.B., Einaudi, M.T. and Kunze, K. (2005): Copper deposition during quartz dissolution by cooling magmatic-hydrothermal fluids: the Bingham porphyry. *Earth and Planetary Science Letters*, 235, 229-243.

Pollard, P.J. (2006): An intrusion-related origin for Cu-Au mineralization in iron oxide-copper-gold (IOCG) provinces. *Mineralium Deposita*, 41, 179-187.

Ramboz, C., Pichavant, M. and Weisbrod, A. (1982): Fluid immiscibility in natural processes: use and misuse of fluid inclusion data in terms of immiscibility. *Chemical Geology*, 37, 29-48.

Ramsay, J.G. (1980): The crack-seal mechanism of rock deformation. *Nature* 284, 135-139.

Roedder, E. (1984): Fluid inclusions. *Reviews in Mineralogy*, 12, 644 p.

Simon, G., Kesler, S.E. and Chryssoulis, S. (1999): Geochemistry and textures of gold-bearing arsenian pyrite, twin Creeks, Nevada: implications for deposition of gold in Carlin-type deposits. *Economic Geology,* 94, 405-422.

Suh, C.E. and Lehmann, B. (2003): Morphology and electron-probe microanalysis of residual gold grains at Dimako, Southeast Cameroon. *Neues Jahrbuch für Mineralogie Monatshefte*, 2003(6), 255-275.

Suh, C.E., Lehmann, B. and Mafany, G.T. (2006): Geology and geochemical aspects of lode gold mineralization at Dimako-Mboscorro, Southeast Cameroon. *Geochemistry: Exploration, Environment, Analysis*, 6, 1 - 15.

Tsige, L. (2006): Metamorphism and gold mineralization of the Kenticha-Katawicha area: Adola belt, southern Ethiopia. *Journal of African Earth Sciences*, 45, 16-32.

Ulrich, T., Günther, D. and Heinrich, C.A. (1999): Gold concentrations of magmatic brines and the metal budget of porphyry copper deposits. *Nature*, 399, 676-679.

Urban, M., Thomas, R., Hurai, V., Koneeny, P. and Chovan, M. (2006): Superdense CO_2 inclusions in Cretaceous quartz-stibnite veins hosted in low-grade Variscan basement of the western Carpathians, Slovakia. *Mineralium Deposita*, 40, 867-873.

Van den Kerkhof, A.M. and Thiery, R. (2001): Carbonic inclusions. *Lithos* 55, 49-68.

Wille, S.E. and Klemd, R. (2004): Fluid inclusion studies of the Abawso gold prospect, near the Ashanti Belt, Ghana. *Mineralium Deposita*, 39, 31- 45.

William-Jones, A.E. and Heinrich, C.A. (2006): Vapour transport of metals and the formation of magmatic-hydrothermal ore deposits. *Economic Geology*, 100, 1287-1312.

Yao, Y. and Robb, L.J. (2000): Gold mineralization in Paleoproterozoic granitoids at Obuasi, Ashanti region, Ghana: ore geology, geochemistry and fluid characteristics. *South African Journal of Geology* 103, 255-278.

Yudovskaya, M.A., Distler, V.V., Chaplygin, I.V., Mokhov, A.V., Trubkin, N.V. and Gorbacheva, S.A. (2006): Gaseous transport and deposition of gold in magmatic fluid: evidence from the active Kudryavy volcano, Kurile Islands. *Mineralium Deposita*, 40, 828-848.

Recieved: 20/10/2008

Accepted: 14/06/2008